Spaced Based Search Coil Magnetometers

G. B. Hospodarsky[1]

[1]Department of Physics and Astronomy, University of Iowa, The University of Iowa, Iowa City, IA, 52242, USA

This article has been accepted for publication and undergone full peer review but has not been through the copyediting, typesetting, pagination and proofreading process which may lead to differences between this version and the Version of Record. Please cite this article as doi: 10.1002/2016JA022565

ABSTRACT:

Search coil magnetometers are one of the primary tools used to study the magnetic component of low frequency electromagnetic waves in space. Their relatively small size, mass, and power consumption, coupled with a good frequency range and sensitivity, make them ideal for spaceflight applications. The basic design of a search coil magnetometer consists of many thousands of turns of wire wound on a high permeability core. When a time-varying magnetic field passes through the coil, a time-varying voltage is induced due to Faraday's law of magnetic induction. The output of the coil is usually attached to a preamplifier, which amplifies the induced voltage and conditions the signal for transmission to the main electronics (usually a low frequency radio receiver). Search coil magnetometers are usually used in conjunction with electric field antenna to measure electromagnetic plasma waves in the frequency range of a few Hz to a few tens of kHz. Search coil magnetometers are used to determine the properties of waves, such as comparing the relative electric and magnetic field amplitudes of the waves, or to investigate wave propagation parameters, such as Poynting flux and wave normal vectors. On a spinning spacecraft, they are also sometimes used to determine the background magnetic field. This paper presents some of the basic design criteria of search coil magnetometers and discusses design characteristics of sensors flown on a number of spacecraft.

INTRODUCTION

Search coil magnetometers are very important in the study of electromagnetic waves in space plasmas. Their good frequency range and sensitivity, along with their small size, mass and power consumption make them ideal for space flight applications. The smaller size and mass of search coil magnetometers more easily allow three-component measurements with good sensitivity compared to electric field antenna elements, which are limited in their length (and thus sensitivity) for the axis parallel to the spin axis on spinning spacecraft, and for all three axis on a non-spinning spacecraft. Figure 1 shows a typical design of a search coil magnetometer. Thousands of turns of fine wire are wound on a high permeability core. The output of the coil is attached to a preamplifier, which amplifies the induced voltage and conditions the signal for transmission to the main electronics (usually a low frequency radio receiver). Search coil magnetometers are usually used in conjunction with electric antennas to measure electromagnetic plasma waves, both naturally occurring waves and also waves generated by ground transmitters. One of the primary reasons to include search coil magnetometers on a spacecraft is to determine the properties of the waves detected, from basic properties such as the ratio of the electric to magnetic components of the wave, to more involved properties, the wave normal and Poynting vectors associated with the waves.

The first magnetometer flown in space by the United States was a search coil magnetometer on Pioneer 1, launched in October 1958 [*Judge et al.*, 1960]. This search coil had an upper frequency limit of a few Hertz and was designed to investigate the magnetic field of Earth, the Moon, and interplanetary space. The first magnetometer flown in space to measure natural plasma wave magnetic fields occurring at higher frequency (>100 Hz), was a loop magnetometer flown on the Injun 3 spacecraft in 1962 [*Gurnett and Obrien*, 1964]. This loop magnetometer had a frequency bandwidth of ~500 to 7000 Hz and was specifically designed to measure very-low-frequency (VLF) electromagnetic waves. The first United

States spacecraft to fly a search coil magnetometer designed to measure VLF waves was OGO-1 launched in 1964 [*Frandsen et al.*, 1969; *Holzer et al.*, 1966]. Since these early missions, loop and search coil magnetometers from many different countries have flown on many different spacecraft, and are included on most new missions that contain a plasma wave instrument. A non-exhaustive list of some of these past spacecraft includes Injun 5 [*Gurnett et al.*, 1969], OGO-2, 3, 4, 5, and 6 [*Frandsen et al.*, 1969], IMP-6, 7 and 8 [*Gurnett*, 1974; *Gurnett and Shaw*, 1973], ISEE-1, -2, and -3 [*Gurnett et al.*, 1978; *Scarf et al.*, 1978], GEOS-1 and -2 [*S-300 Experimenters*, 1979], Dynamics Explorer (DE) 1 [*Shawhan et al.*, 1981], Geotail [*Hayashi*, 1988], Viking [*Hultqvist*, 1990], FREJA [*Holback et al.*, 1994], Polar [*Gurnett et al.*, 1995], Cluster [*Cornilleau-Wehrlin et al.*, 1997], DEMETER [*Séran and Fergeau*, 2005], THEMIS [*Roux et al.*, 2008], Van Allen Probes [*Kletzing et al.*, 2013a], and Magnetospheric Multiscale (MMS) [*Le Contel et al.*, 2016]. Search coil magnetometers have also been flown on spacecraft that have orbited Jupiter (Galileo [*Gurnett et al.*, 1991] and Juno), Saturn (Cassini [*Gurnett et al.*, 2004]), and investigated the solar wind (Helios [*Neubauer et al.*, 1977], Ulysses [*Stone et al.*, 1992], and Wind [*Bougeret et al.*, 1995]).

The primary difference between loop and search coil magnetometers is that the search coil usually employs a high permeability magnetic core to concentrate the magnetic flux in a coil made up of many thousands of turns of wire (see Figure 1). However, the finite frequency response of the permeable core material limits this concentration at high frequencies. This difference leads to space-based loop magnetometers usually having larger frequency bandwidths (upper frequency cutoff usually in the 100's of kHz), but poorer low frequency (<1 kHz) sensitivity than search coil magnetometers, which typically have upper frequency cutoffs <10 kHz, but good sensitivity at lower frequencies. However, there have been search coils designed to measure higher (>100 kHz) frequencies (e.g. AMPTE [*Hausler et al.*, 1985] and INTERBALL-2 [*Lefeuvre et al.*, 1998]). Loop magnetometers also tend to

be larger in size and mass compared to search coil magnetometers, especially if all three axis magnetic components are to be measured. See *Gurnett* [1998] for a detailed discussion of loop magnetometers and the performance and design trade-offs between space-based loop and search coil magnetometers.

SEARCH COIL MAGNETOMETER BASIC DESIGN CRITERIA

Search coil antenna work due to Faraday's law of magnetic induction, which states that a loop of wire with a time-varying magnetic field passing through it will have a time-varying voltage induced around it. This induced voltage (V) is proportional to the time rate of change of the magnetic field and can be written as

$$V = -c\frac{d}{dt}(\mathbf{B} \cdot \hat{\mathbf{n}}) \quad (1)$$

where c is a constant that depends on the area of the loop and on the properties of the core material, **B** is the magnetic field vector, and **n** is the unit vector along the axis of the coil. The time varying magnetic field experienced by the coil can be due to temporal variations of the field, or if the coil is in motion, spatial variations of the field. The induced voltage can be rewritten as

$$V = -c[\mathbf{B} \cdot \frac{\boldsymbol{dn}}{\boldsymbol{dt}} + \mathbf{n} \cdot \frac{\boldsymbol{dB}}{\boldsymbol{dt}} + \mathbf{u} \cdot \boldsymbol{\nabla}[\mathbf{B} \cdot \mathbf{n}]]. \quad (2)$$

The first term represents the voltage induced by the angular motion of the coil, and is the primary term used by the search coils on spinning spacecraft to measure the background DC magnetic field. The third term represents the convective motion of a coil with velocity **u** relative to the magnetic field **B**. The second term is the one that is most important in the study of the magnetic component of electromagnetic waves. In most space environments, the first and third terms are negligible or can be filtered out due to their low frequency, and can be ignored.

For a typical search coil magnetometer, made up of a ferromagnetic core enclosed by a solenoidal coil of N turns of wire, the induced voltage can be written as

$$V = -NA\mu_e(\frac{dB}{dt}) \quad (3)$$

where A is the cross-sectional area of the core, μ_e is the effective permeability of the core, and $(\frac{dB}{dt})$ is the time variation of the magnetic field component parallel to the coil axis. If the variation of the magnetic field is sinusoidal, the equation reduces to

$$V = -2\pi NA\mu_e f B_o x 10^{-7} \mu V \quad (4)$$

where B_o is the amplitude of the magnetic signal in nT, A is in cm^2, and f is the frequency of the time variation.

The above analysis assumes that the coil is a pure inductor, but real search coil magnetometers have a resistance due to the resistivity of the wire, and a capacitance due to the self-capacitance between the turns in the coil. These additional factors can be modeled using the equivalent circuit shown in Figure 2. The induced voltage due to the time varying magnetic field is represented by a voltage source in series with an inductor (L). A resistance (R_1) is in series with L. This resistance includes the resistance of the wire (including skin effects at higher frequencies), and any losses due to eddy currents and hysteresis in the core material. In most cases, the resistance of the wire is much larger than the other possible contributions, and these other losses can be neglected. The self-capacitance (C) due to the potential difference between adjacent turns and layers of the coils is parallel to L and R_1. A damping resistor (R_D) represents the input impedance (both resistive and reactive) of the preamplifier and controls the sharpness of the resonant peak of a coil without flux feedback. An analysis of this equivalent circuit modifies Equation 4 to

$$V = \frac{-2\pi NA\mu_e f B_o \, x \, 10^{-7} \mu V}{\sqrt{\left(1+\frac{R_1}{R_D}-\omega^2 LC\right)^2+\left(\frac{\omega L}{R_D}+\omega C R_1\right)^2}} \quad (5)$$

where $\omega = 2\pi f$. For typical values of L, C, R_1, and R_D, the denominator is ≈1 for ω well below $\omega_r = 1/\sqrt{LC}$, where $\omega_r/2\pi$ is called the resonance frequency (f_r). Search coils are usually designed with a resonant frequency above the expected measurement frequency range. Figure 3 shows the comparison of the theoretical transfer function (Equation 5) for the measured values of R_1, R_D, L, and C of the Wind search coils (solid line) vs. the measured transfer function (circles) [*Hospodarsky*, 1992].

As Figure 3 shows, Equation 5 can accurately predict the output voltage of a search coil magnetometer if the values of the components of the equivalent circuit in Figure 2 can be estimated or measured. However, the amplitude response over frequency is just one component of a search coil response to the input magnetic field emission. The relative phase response over frequency of the sensor and electronics are also needed if certain wave propagation parameters, such as Poynting vector and polarization, are to be determined. Modeling the relative phase shift between the input magnetic field and the output voltage from the preamplifier is much more difficult, and is usually best determined through tests and calibrations. Figure 4 shows the measured phase shift between the input magnetic field and the output voltage of the Van Allen Probes search coil sensor and preamplifier.

The real part of the impedance of the equivalent circuit is important in determining the noise level of the search coil since it determines the thermal noise (or Johnson noise) voltage of the coil. The real part of the impedance (Z_r) of the circuit in Figure 2 is

$$Z_r = \frac{R_1\left(1+\frac{R_1}{R_D}-\omega^2 LC\right)+\omega L\left(\frac{\omega L}{R_D}+\omega C R_1\right)}{\left(1+\frac{R_1}{R_D}-\omega^2 LC\right)^2+\left(\frac{\omega L}{R_D}+\omega C R_1\right)^2}\ ohms \qquad (6)$$

The real part of the impedance ranges from ~R_1 ohms at low frequencies to ~R_D ohms near the resonant frequency. The Johnson noise voltage (V_J) for a frequency bandwidth (Δf) of a search coil is given by [*Robinson*, 1974] as

$$\frac{V_J}{\sqrt{\Delta f}} = \sqrt{4k_B T Z_r}\ \frac{Volts}{\sqrt{Hz}} \qquad (7)$$

where k_B is Boltzmann constant and T is the temperature in degrees Kelvin.

The noise level of a search coil is usually defined as the magnetic signal strength that induces a voltage equal to the noise voltage. Setting the noise voltage from Equation 7 equal to the output voltage due to a magnetic field signal from Equation 5, solving for the magnetic signal and squaring both sides gives

$$\frac{B_N^2}{\Delta f} \cong \frac{4k_B T}{(\omega N A \mu_e \text{ x } 10^{-7})^2}\left(R_1 + \frac{R_1^2}{R_D} + \frac{\omega^2 L^2}{R_D}\right)\frac{nT^2}{Hz} \qquad (8)$$

which has units of magnetic field spectral density. The noise level estimates the minimum magnetic signal a search coil magnetometer can measure in a given frequency bandwidth. For typical search coil magnetometers, the values of R_1 and R_D are such that $R_1 << R_D$, so Equation 8 can be rewritten as

$$\frac{B_N^2}{\Delta f} \cong \frac{4k_B T}{(N A \mu_e \text{ x } 10^{-7})^2}\left(\frac{R_1}{\omega^2} + \frac{L^2}{R_D}\right)\frac{nT^2}{Hz} \qquad (9).$$

Including the noise level voltage of a preamplifier in Equation 8 and again using the typical values for L, C, R_1, and R_D gives

$$\frac{B_N^2}{\Delta f} \cong \frac{1}{(N A \mu_e \text{ x } 10^{-7})^2}\left[4k_B T\left(\frac{R_1}{\omega^2} + \frac{L^2}{R_D}\right) + \frac{n_{amp}^2/\Delta f}{\omega^2}\right]\frac{nT^2}{Hz} \qquad (10)$$

where $n^2_{amp}/\Delta f$ is the voltage noise spectral density of the preamplifier. As Equation 10 shows, the noise of preamplifier can play an important role in the overall noise level of the search coil magnetometer, especially at low frequencies. For the noise level of the coil itself, the resistance of the wire determines the noise level at low frequencies, but at higher frequencies, L^2/R_D usually dominates. A good search coil magnetometer design uses the optimum combination of the above variables to minimize the noise level in the frequency range of interest.

Many search coils have included a flux feedback method to flatten the frequency response of the sensor over the measurement frequency range of interest. This flattening usually makes the sensor more stable over temperature and is especially useful in simplifying the calibration of the sensor over frequency. For example, if time-series waveform measurements are obtained, a flat frequency response removes the difficulty of calibrating the waveform over much of the frequency range. However, it is usually not possible to flatten the entire expected measurement frequency range of the sensor, especially the lower frequencies. The flux feedback is usually accomplished by using a separate feedback winding on the core and has been used on a number of missions (e.g. GEOS-1 and -2 [*S-300 Experimenters*, 1979], Geotail [*Hayashi*, 1988], Galileo [*Gurnett et al.*, 1991], Ulysses [*Stone et al.*, 1992], Cluster [*Cornilleau-Wehrlin et al.*, 1997], Cassini [*Gurnett et al.*, 2004], DEMETER [*Séran and Fergeau*, 2005], THEMIS [*Roux et al.*, 2008], and Magnetospheric Multiscale (MMS) [*Le Contel et al.*, 2016]. The flattening of the frequency response of the sensor can also be accomplished using current feedback system in the preamplifier [*Tumanski*, 2007]. The recently launched Juno and Van Allen Probes search coils [*Kletzing et al.*, 2013a] are examples of a current feedback circuit in the preamplifier used to flatten the response of the sensor instead of a secondary winding.

SEARCH COIL MAGNETOMETER DESIGN CONSIDERATIONS:

Effective Permeability (μ_e)

The effective permeability of the core affects the sensitivity and noise level of the search coil as shown in Equation 3 and 10, specifically the larger the value for μ_e, the larger voltage out of the sensor and the lower the noise level. The determination of μ_e is difficult and depends both on the material and shape of the core. Magnetic materials are usually rated

according to their closed loop permeability (μ_i), where closed loop permeability is defined as the ratio of the magnetic flux density in the material compared to the ambient magnetic field density present in the absence of the material. However, since search coil magnetometers usually employ a bar made up of laminated strips or a number of thin rods bundled together, the effective permeability is less than the closed-loop permeability by which ferromagnetic materials are rated [*Bozorth and Chapin*, 1942]. The effective permeability of a long bar or rod is primarily determined by the length (*l*) to diameter (d) ratio of the core. For a core material with $\mu_i >> 1$ and *l*>>d, *Hayashi* [1988] found

$$\mu_e \approx \frac{1}{D_B\left(1-\frac{1}{\mu_i}\right)+\frac{1}{\mu_i}} \tag{11}$$

where D_B is the demagnetizing factor determined from

$$D_B = \frac{\ln\left(\frac{3\ell}{2d}\right)-1}{\left(\frac{\ell}{d}\right)^2} \tag{12}$$

These equations gives the theoretical value of μ_e at the center of the rod, but the effective permeability is known to decrease as one approaches the ends of the rods [*Bozorth and Chapin*, 1942]. *Hill* [1962] derives the following function of μ_e verses the distance from the center of the rod

$$\mu_{e(x)} = \mu_{e(center)}\left(1 - 3.8\frac{x^2}{l^2}\right) \tag{13}$$

where $\mu_{e(center)}$ is the effective permeability at the mid-point of the core determined from Equation 11 and *x* is the distance from the center of the core. Equation 13 shows that the largest effective permeability is achieved for coils located near the center of the core. Equation 11 also shows that a larger *l*/d ratio produces a larger μ_e. However, the effective permeability for very large *l*/d ratios (> 100) can be sensitive to temperature changes and mechanical stresses. Also, there are size and weight limits for search coil magnetometers designed for space applications which restrict the length of the core.

Because the effective permeability is integral in determining the sensitivity and noise level of a search coil magnetometer, a number of efforts have been made to develop unique core shape and designs to increase search coil performance [*Coillot et al.*, 2014; *Coillot et al.*, 2007]. A recent example of this effort are the search coils flown on the MMS spacecraft [*Le Contel et al.*, 2016], which employ magnetic concentrators at the end of their ferromagnetic core to increase the effective permeability. Another attempt to increase search coil performance used on the DEMETER mission was to concentrate the largest number of the coil windings at the center of the core, providing the maximum sensitivity for the total number turns needed for the frequency range of interest [*Séran and Fergeau*, 2005].

Resistance of the Wire

The resistance of the coil depends primarily on the length, diameter, and type of the wire.

For a cylindrical core with N turns of wire, the resistance can be estimated by

$$R \approx 2\pi r_{mean} N\rho \qquad (14)$$

where r_{mean} is the mean radius of the winding, ρ is the resistance per unit length, and N is the number of turns. Because the core of a search coil is often constructed of laminated strips of high permeable material resulting in a square cross sectional area, the wire of the coil is often wound on a square bobbin. The resistance of the wire for a square bobbin is given by

$$R = 4(a + 0.7854D)N\rho \ \ ohms \qquad (15)$$

where a is the inner width of the bobbin and D is the depth of the winding [*Underhill*, 1910]. The material and diameter of the wire determine ρ. For a given number of turns, the mean radius and depth of the windings also depend on the diameter of the wire. From Equation 10 we can see that the resistance of the wire should be kept as small as possible in order to minimize the noise level of the search coil. This minimization is accomplished by choosing

the largest diameter wire that will fit on the bobbin for a given number of turns and which also fits within the mass limit of the sensor.

Inductance

The inductance of a solenoid on a high permeability core can be estimated from the following formula [Parady, 1974]

$$L = \frac{\mu_o \mu_e N^2 A}{\ell} \qquad (16)$$

where μ_o is the permeability constant, μ_e is the effective permeability of the core, A is the cross-sectional area of the core in square meters, N is the number of turns, and *l* is the length of the core in meters. It should be noted that the inductance varies with the square of the number of turns and is proportional to μ_e. As the resonant frequency is proportional to the inverse of the square root of the inductance, the resonant frequency is proportional to the inverse of the number of turns and also to the inverse of the square root of μ_e. This relationship leads to a trade off as more turns leads to a better sensitivity, but decreases the bandwidth of the search coil.

Capacitance

The capacitance of a search coil is often difficult to model, as the method of winding the coil has a large effect on the final capacitance [*Welsby*, 1960]. Also, capacitance from the wires connecting the coil to the preamplifier, or in the preamplifier itself can also play a large role. An estimate for the capacitance of one section of a multi-section coil is given by Hill [1962]

$$C = \frac{0.00381 \pi r_1 \epsilon_r W}{(K_1 - 1) d\lambda} \qquad (17)$$

where r_1 is the mean radius of the coil, W is the width of the coil, ε_r is the average dielectric constant of the insulation on the wire, K_1 is the ratio of the distance between the center of two adjacent wires and the diameter of the wire (d), and λ is the number of layers of wire.

Equation 5 shows that for a large resonant frequency, it is desirable for the capacitance to be as small as possible. One way to accomplish a lower capacitance is to split the coil into smaller sections separated by a small gap. If a coil that originally had a capacitance C, is split into n sections, each section would have a capacitance ~C/n. These sections are connected in series, which gives a new capacitance of C/n^2 for the entire search coil. There is also a capacitance between the sections, which when taken into account, gives a total capacitance of

$$C_{tot} = \frac{C}{n^2} + \frac{C_1}{(n-1)} \qquad (18)$$

where C_1 is the capacitance between adjacent sections. As we want C_{tot} to be smaller than the original unsegmented coil capacitance, C_1 should be kept small which can be accomplished by having a large enough space between the sections. There is a limit to the effectiveness of splitting the coils. If n is small, C_{tot} varies inversely to n^2, but as n becomes large, the $C_1/(n-1)$ term starts to dominate and the resistance of the wire increases as the number of sections are increased, which raises the noise level of the search coil as seen from Equation 9. There is also a size limit on a search coil to be flown in space, which limits both the number of sections, and the space between each section.

Damping Resistor

The damping resistor plays an important role in the sensitivity and noise level of the search coil as shown in Equations 5 and 10. The damping resistor can be an actual resistor placed in parallel with the coils, the input impedance of the preamplifier, or a combination of the two.

Noise and Noise Sources

The ability for search coil magnetometers to measure weak signals is determined by the amount of noise present. Noise is the unwanted signal that obscures the desired signal. There are various types and sources of noise. Some of the most important ones are the Johnson noise due to the resistance of the wire in the coil, noise in the preamplifier (as shown in Equations 8 and 10), as well as interference from outside sources. Johnson noise, also known as Nyquist noise or thermal noise, is the noise found in any material with a resistance. It is caused by the random motion of the free electrons in the material. This random motion produces small instantaneous potential differences between the ends of the material. Since the noise voltage is random, it has a flat frequency spectrum, and is often called "white noise." For a resistor with resistance R, it is usually written as shown in Equation 7 with R replacing the real part of the impedance Z_r [*Robinson*, 1974].

Another type of noise found in a search coil magnetometer is noise produced in the preamplifier. This noise is usually made up of two main components, 1/f, and Johnson noise. The 1/f noise usually dominates at low frequencies, while Johnson noise dominates at higher frequencies [*Horowitz and Hill*, 1980]. As shown in Equation 10, the noise of preamplifier can play an important role in the overall noise level of the search coil magnetometer, and should be designed to be as quiet as possible within the resource (usually size and power) limits.

The other type of noise important in the performance of space-based search coil magnetometers is interference from the spacecraft, other instruments, or interference during testing and calibration on the ground. The interference most often encountered in the lab with a search coil magnetometer is interference from power lines (60 Hz and harmonics in the United States). Other sources of interference can be from other electron devices and

computer monitors, usually in the tens of kHz range, and signals from radio stations, 540 kHz and above. This interference must be reduced or removed to allow a good calibration of the sensor and is usually accomplished by performing the calibration inside of magnetic shielding or at a calibration site that is magnetically clean.

While in space, electrical interference from the spacecraft or other instruments can also increases the noise level and obscures the natural signals the sensor is trying to measure. Various steps can and should be taken to reduce magnetic interference. Magnetometers should be deployed as far from the spacecraft body as possible. Most interference fields are dipole in nature and vary as $1/r^3$, where r is the distance between the noise source and the sensor. If r is large, then the interference will be reduced, hopefully below the noise level of the search coil. For this reason, search coil magnetometers are often mounted on the end of a many meter boom, far from the spacecraft main electrical systems. Current carrying wires should also be twisted in pairs and large current loops in the spacecraft harness design should be avoided. Any current loops that are necessary should be made as small as possible to minimize the magnetic moment.

Power converters should operate at the highest possible frequency, preferably well above the frequency range of the sensor. Shielding can also reduce magnetic interference, but due to weight considerations, shielding can only be applied to small components or areas of the spacecraft. At spacecraft level testing and calibration, each instrument should be tested individually with the search coil magnetometers to examine its possibility for generating interference.

To illustrate the importance of the various noise sources discussed above, Figure 5 shows the noise level of nine different search coil designs that have flown in space over the last ~50 years. As can be seen the noise level of a search coil can vary greatly depending on

the search coil design and the requirements of the mission. The next section will examine in more detail some of these search coil designs and the reasons for this variation.

EXAMPLES OF SPACE BASED SEARCH COIL MAGNETOMETERS

Polar and Wind Search Coils

The Polar and Wind spacecraft were part of the NASA Global Geospace Science (GGS) International Solar Terrestrial Physics (ISTP) Program [*Acuña et al.*, 1995]. The Wind spacecraft was launched in 1994 to measure the solar wind in the vicinity of Earth and is still operating as of mid-2016. The Polar spacecraft was launched in 1996 to study Earth's polar magnetosphere and aurora, and operated until April 2008. The search coils for the Wind WAVES Instrument [*Bougeret et al.*, 1995] and the Polar Plasma Wave Investigation (PWI) [*Gurnett et al.*, 1995] were built at the University of Iowa and loosely based on earlier search coil designs flown on the International Sun-Earth Explorer (ISEE) spacecraft [*Gurnett et al.*, 1978; *Scarf et al.*, 1978], but with a number of design changes to improve their performance.

The search coils for both spacecraft had the same basic design with two separate bobbins of wire on a high permeable core with the preamplifier located between the coils. The cores consisted of a 4 mil Supermalloy laminated bar with dimensions of 0.48 x 0.48 x 39.4 cm. The edge of the bobbins were positioned 3.24 cm from the center of the core and each bobbin contained eight sections containing the wire, seven of which contain the primary windings, and one that contains a calibration winding. The Polar search coils contained 10.010 turns of #40 American Wire Gauge (AWG) wire per bobbin, resulting in a resonance frequency of ~10,000 Hz. The Wind search coils were optimized for the lower frequency plasma wave observations expected in the solar wind. Each Wind bobbin contained 40,005

turns of #44 AWG wire per bobbin, resulting in a resonance frequency of ~1600 Hz (see Figure 3). The Polar and Wind search coils also contained a calibration winding of 1000 turns of #40 AWG wire in the eighth section.

A number of changes [*Hospodarsky*, 1992] in the Polar and Wind search coil sensor and preamplifier designs reduced the noise level by ~√2 compared to the earlier ISEE search coil designs [*Gurnett et al.*, 1978; *Scarf et al.*, 1978]. This difference in noise level is shown in Figure 5. Above 200 Hz the Polar search coil noise level (red line) is approximately √2 times lower than the ISEE-2 noise levels (red dashed line).

Juno and Van Allen Probe Search Coils

The New Frontiers Juno spacecraft was launched on August 5, 2011 to study Jupiter's composition, magnetic field, gravity field, and polar magnetosphere. The spacecraft arrived at Jupiter on July 5, 2016 and is expected to complete at least 37 polar orbits during its nominal mission. Juno will be the first spacecraft to explore in situ the near (~4300 km) Jovian polar region [*Bagenal et al.*, 2014]. The Juno spacecraft includes the Waves instrument which includes an electric dipole antenna and a single search coil magnetometer.

The Van Allen Probes mission consists of two identical spacecraft that were launched on August 30, 2012 to study Earth's Van Allen radiation belts [*Mauk et al.*, 2013]. The spacecraft include the Electric and Magnetic Fields Instrument Suite and Integrated Science (EMFISIS) suite [*Kletzing et al.*, 2013a]. EMFISIS includes a triaxial magnetometer (MAG) and a plasma wave instrument (Waves), which includes a triaxial search coil (MSC).

The designs of the Juno and Van Allen Probes search coils have many similarities due to their near simultaneous construction, their similar expected measurement frequency range, and the expected high radiation environments encountered by both missions. Both designs consists of a single bobbin with eight sections and 10,000 total turns of #38 wire located at

the center of a high permeable core. The Van Allen Probe core length is ~40 cm, similar to the Polar and Wind cores. The Juno core length is only ~15 cm, much shorter than the Van Allen Probes core. The Juno core was shortened to reduce the possible variable field produced by soft magnetic core material on the spacecraft that could be detected by the Juno Magnetometer instrument (MAG). The shorter core also reduces sensitivity of the search coil at lower frequencies, preventing the sensor from saturating near perigee due to the spinning spacecraft encountering the very large (~12 Gauss) Jovian background magnetic field. This reduction in the sensitivity caused by the much shorter core compared to Van Allen Probes can be seen in Figure 5 and 6.

Both missions use the same low noise preamplifier design. The preamplifiers are designed to survive a heavy radiation environment. The preamplifiers supply a feedback current to the main coils to flatten the voltage response over frequency as shown in Figure 6. The small bump at ~10,000 Hz is due to the feedback circuit imperfectly flattening the voltage response at the resonance frequency of the sensor coil. The Van Allen Probes Search Coils are mounted on a boom about four meters from center of spacecraft in a tri-axial configuration with the three preamplifiers stacked in the main cylindrical housing and the three search coil sensors (coil and core) mounted perpendicular to each other and parallel to the three electric antenna axes (see *Kletzing et al.* [2013a] for details and a picture of the Van Allen Probes search coil assembly). The Van Allen Probe search coils measure a frequency range of a few Hz to ~12 kHz and are qualified for an operating temperature range of -70 to +35 C. Figure 5 shows the noise level of one of the Van Allen Probes search coils (green dashed line) as measured before integration on the spacecraft as compared to the Juno (green line) and number of other search coils.

The Juno search coil is a single axis coil which is body mounted (no boom) to the spacecraft. This mounting choice was done to reduce mass, cost, and to keep the search coil

magnetic core farther away from the Juno MAG instrument. As discussed earlier, body mounting a search coil to the spacecraft is not ideal, as it increases the likelihood of detecting spacecraft interference. However the Juno spacecraft and instruments had a strong pre-launch electromagnetic control plan to limit the amount of noise emitted from the spacecraft in the frequency range of the Juno search coil. This can be seen by the green line in Figure 5 which shows the in-flight noise level of the Juno search coil.

MMS Search Coils

The Magnetospheric Multiscale mission [*Burch et al.*, 2016] consists of four spacecraft launched on March 12, 2015 and designed to fundamentally increase our understanding of magnetic reconnection, particle acceleration and turbulence. The MMS FIELDS instrument suite [*Torbert et al.*, 2016] includes a 3-axis search coil magnetometer SCM [*Le Contel et al.*, 2016] on each spacecraft. The MMS search coils were designed and built by the Laboratoire de Physique des Plasmas (LPP) and are loosely based on the Cluster [*Cornilleau-Wehrlin et al.*, 1997] and THEMIS [*Roux et al.*, 2008] search coils. The MMS SCM were designed to meet the specific science requirements of the MMS mission, taking into account the limited mass allocation available for the SCM. Also, due to the large field strengths that were expected to be encountered in the reconnection regions, a very sensitive (low noise floor) search coil sensor was not required. These allocation limitations and science requirements lead to an optimized search coil design with a tri-axial sensor configuration located on a boom 4 meters from the spacecraft and the preamplifier box mounted on the spacecraft near the base of the boom. Each sensor consist of a 10 cm long core shaped in a way to produce magnetic amplification [*Coillot et al.*, 2014; *Coillot et al.*, 2007]. The coils contain of over 10,000 turns of wire and a flux feedback winding is used to

flatten the output response of the sensor. The MMS SCM has a nominal frequency range of ~1 Hz to 6 kHz.

The noise level of the MMS SCM is shown on Figure 5 (blue dashed line). As can be seen, the noise level of the MMS SCM is very similar to that of Juno (green line) up to ~1500 Hz, and both are higher than most of the other sensors shown on Figure 5. It should be remembered that both Juno and MMS SCM were designed to meet the specific science requirements of their mission, and each have a much shorter core (15 cm for Juno, 10 cm for MMS) than the other search coils. As Equations 5, 10 and 11 show, the length of the core affects both the sensitivity and noise level of a search coil, leading to the higher noise levels.

CONCLUSION

Search coil magnetometers are one of the primary tools used to measure wave magnetic fields in the frequency range of a few Hz to ~10 kHz. A number of basic design criteria are true for almost all search coil designs. However, various modifications and tweaks have been used on a number of missions in attempts to improve sensitivity and noise level, or to meet specific science goals. Exciting new ideas and designs are being investigated and planned for future space missions. One interesting new design is the Dual-Band Search Coil Magnetometer that allows two different frequency ranges (few kHz for one, tens or hundreds of kHz for the other) to be measured with a single sensor [*Coillot et al.*, 2010]. This design is planned to be flown on the Solar Probe Plus mission to study the sun the BepiColombo mission to Mercury [*Kasaba et al.*, 2010]. The BepiColombo missions employs a compound system of two single band, lower frequency (0.1 Hz and 20kHz) search coils (LF-SC) in the spin plane of the spacecraft, and a dual band (0.1 Hz to 20kHz and 10 to 640 kHz) search coil (DB-SC) aligned with the spin axis. This design shows that advances are still being made in a sensor that has been used since the early days of the space program.

Acknowledgements. The research at The University of Iowa was supported by JHU/APL contract no. 921647 under NASA Prime contract no. NAS5-01072 and by SwRI contract 6999041X. This work contains no new scientific data.

References:

Acuña, M. H., K. W. Ogilvie, D. N. Baker, S. A. Curtis, D. H. Fairfield, and W. H. Mish (1995), The Global Geospace Science Program and its investigations, *Space Sci Rev*, *71*(1), 5-21, doi:10.1007/bf00751323.

Bagenal, F., et al. (2014), Magnetospheric Science Objectives of the Juno Mission, *Space Sci Rev*, 1-69, doi:10.1007/s11214-014-0036-8.

Bougeret, J.-L., et al. (1995), WAVES: The radio and plasma wave investigation on the wind spacecraft, *Space Sci Rev*, *71*(1), 231-263, doi:10.1007/bf00751331.

Bozorth, R. M., and D. M. Chapin (1942), Demagnetizing Factors of Rods, *Journal of Applied Physics*, *13*(5), 320-326, doi:doi:http://dx.doi.org/10.1063/1.1714873.

Burch, J. L., T. E. Moore, R. B. Torbert, and B. L. Giles (2016), Magnetospheric Multiscale Overview and Science Objectives, *Space Sci Rev*, *199*(1), 5-21, doi:10.1007/s11214-015-0164-9.

Coillot, C., J. Moutoussamy, M. Boda, and P. Leroy (2014), New ferromagnetic core shapes for induction sensors, *J. Sens. Sens. Syst.*, *3*(1), 1-8, doi:10.5194/jsss-3-1-2014.

Coillot, C., J. Moutoussamy, R. Lebourgeois, S. Ruocco, and G. Chanteur (2010), Principle and Performance of a Dual-Band Search Coil Magnetometer: A New Instrument to Investigate Fluctuating Magnetic Fields in Space, *Sensors Journal, IEEE*, *10*(2), 255-260, doi:10.1109/JSEN.2009.2030977.

Coillot, C., J. Moutoussamy, P. Leroy, G. Chanteur, and A. Roux (2007), Improvements on the design of search coil magnetometer for space experiments, *Sensor Letters*, *5*, 167-170.

Cornilleau-Wehrlin, N., et al. (1997), The Cluster Spatio-Temporal Analysis of Field Fluctuations (STAFF) Experiment, *Space Sci Rev*, *79*(1), 107-136, doi:10.1023/a:1004979209565.

Frandsen, A. M., R. E. Holzer, and S. E. J. (1969), OGO Search Coil Magmetometer Experiments, *IEEE Transactions on Geoscience Electronics*, *GE-7*(No. 2).

Gurnett, D. A. (1974), Earth as a Radio-Source - Terrestrial Kilometric Radiation, *Journal of Geophysical Research*, *79*(28), 4227-4238, doi:DOI 10.1029/JA079i028p04227.

Gurnett, D. A. (1998), Principles of Space Plasma Wave Instrument Design, in *Measurement Techniques in Space Plasmas Fields*, edited, pp. 121-136, American Geophysical Union, doi:10.1002/9781118664391.ch14.

Gurnett, D. A., et al. (2004), The Cassini radio and plasma wave investigation, *Space Sci Rev*, *114*(1-4), 395-463, doi:DOI 10.1007/s11214-004-1434-0.

Gurnett, D. A., W. S. Kurth, A. Roux, R. Gendrin, C. F. Kennel, and S. J. Bolton (1991), Lightning and Plasma-Wave Observations from the Galileo Flyby of Venus, *Science*, *253*(5027), 1522-1525, doi:DOI 10.1126/science.253.5027.1522.

Gurnett, D. A., and B. J. Obrien (1964), High-Latitude Geophysical Studies with Satellite Injun 3 .5. Very-Low-Frequency Electromagnetic Radiation, *Journal of Geophysical Research*, *69*(1), 65-&, doi:DOI 10.1029/JZ069i001p00065.

Gurnett, D. A., et al. (1995), The Polar Plasma-Wave Instrument, *Space Sci Rev*, *71*(1-4), 597-622, doi:Doi 10.1007/Bf00751343.

Gurnett, D. A., G. W. Pfeiffer, R. R. Anderson, S. R. Mosier, and D. P. Cauffman (1969), Initial Observations of Vlf Electric and Magnetic Fields with Injun-5 Satellite, *Journal of Geophysical Research*, *74*(19), 4631-&, doi:DOI 10.1029/JA074i019p04631.

Gurnett, D. A., F. L. Scarf, R. W. Fredricks, and E. J. Smith (1978), Isee-1 and Isee-2 Plasma-Wave Investigation, *Ieee T Geosci Remote*, *16*(3), 225-230, doi:Doi 10.1109/Tge.1978.294552.

Gurnett, D. A., and R. R. Shaw (1973), Electromagnetic Radiation Trapped in Magnetosphere above Plasma Frequency, *Journal of Geophysical Research*, *78*(34), 8136-8149, doi:DOI 10.1029/JA078i034p08136.

Hausler, B., et al. (1985), The Plasma-Wave Instrument on Board the Ampte Irm Satellite, *Ieee T Geosci Remote*, *23*(3), 267-273, doi:Doi 10.1109/Tgrs.1985.289526.

Hayashi, K. (1988), Improvement of the Tri-Axial Search Coils Onboard Geotail Satellite and Electromagnetic Interference (EMI) Problem on the Satellite, PhD thesis, Kanazawa University, Kanazawa, Japan.

Hill, L. K. (1962), Micropulsation Sensors with Laminated MUMETAL Cores, PhD thesis, The University of Texas, Austin, Texas, USA.

Holback, B., S.-E. Jansson, L. Åhlén, G. Lundgren, L. Lyngdal, S. Powell, and A. Meyer (1994), The Freja wave and plasma density experiment, *Space Sci Rev*, *70*(3), 577-592, doi:10.1007/bf00756887.

Holzer, R. E., M. G. McLeod, and E. J. Smith (1966), Preliminary results from the Ogo 1 Search Coil Magnetometer: Boundary positions and magnetic noise spectra, *Journal of Geophysical Research*, *71*(5), 1481-1486, doi:10.1029/JZ071i005p01481.

Horowitz, P., and W. Hill (1980), *The Art of Electronics*, Cambridge University Press, Cambridge.

Hospodarsky, G. B. (1992), Search Coil Magnetometers for the ISTP Polar and Wind Spacecraft, MS thesis, University of Iowa, Iowa City, Iowa, USA.

Hultqvist, B. (1990), The Swedish Satellite Project Viking, *Journal of Geophysical Research: Space Physics*, *95*(A5), 5749-5752, doi:10.1029/JA095iA05p05749.

Judge, D. L., M. G. McLeod, and A. R. Sims (1960), The Pioneer I, Explorer VI and Pioneer V High-Sensitivity Transistorized Search Coil Magnetometer, *Space Electronics and Telemetry, IRE Transactions on*, *SET-6*(3-4), 114-121, doi:10.1109/IRET-SET.1960.5008730.

Kasaba, Y., et al. (2010), The Plasma Wave Investigation (PWI) onboard the BepiColombo/MMO: First measurement of electric fields, electromagnetic waves, and radio waves around Mercury, *Planetary and Space Science*, *58*(1–2), 238-278, doi:http://dx.doi.org/10.1016/j.pss.2008.07.017.

Kletzing, C. A., et al. (2013a), The Electric and Magnetic Field Instrument Suite and Integrated Science (EMFISIS) on RBSP, *Space Sci Rev*, *179*(1-4), 127-181, doi:10.1007/s11214-013-9993-6.

Kletzing, C. A., et al. (2013b), The Electric and Magnetic Field Instrument Suite and Integrated Science (EMFISIS) on RBSP, *Space Sci Rev*, *179*(1-4), 127-181, doi:10.1007/s11214-013-9993-6.

Le Contel, O., et al. (2016), The Search-Coil Magnetometer for MMS, *Space Sci Rev*, *199*(1), 257-282, doi:10.1007/s11214-014-0096-9.

Lefeuvre, F., M. Parrot, J. L. Rauch, B. Poirier, A. Masson, and M. Mogilevsky (1998), Preliminary results from the MEMO multicomponent measurements of waves on-board INTERBALL 2, *Ann. Geophys.*, *16*(9), 1117-1136, doi:10.1007/s00585-998-1117-3.

Mauk, B. H., N. J. Fox, S. G. Kanekal, R. L. Kessel, D. G. Sibeck, and A. Ukhorskiy (2013), Science Objectives and Rationale for the Radiation Belt Storm Probes Mission, *Space Sci Rev*, *179*(1-4), 3-27, doi:10.1007/s11214-012-9908-y.

Neubauer, F. M., H. J. Beinroth, H. Barnstorf, and G. Dehmel (1977), Initial Results From HELIOS-1 Search-Coil Magnetometer Experiment, *Journal of Geophysics-Zeitschrift Fur Geophysik*, *42*(6), 599-614.

Robinson, F. N. H. (1974), *Noise and Fluctuations in Electronic Devices and Circuits*, Oxford University Press, London.

Roux, A., O. Le Contel, C. Coillot, A. Bouabdellah, B. Porte, D. Alison, S. Ruocco, and M. C. Vassal (2008), The Search Coil Magnetometer for THEMIS, *Space Sci Rev*, *141*(1), 265-275, doi:10.1007/s11214-008-9455-8.

S-300 Experimenters (1979), Measurements of electric and magnetic wave fields and of cold plasma parameters on-board GEOS-1. Preliminary results, *Planetary and Space Science*, *27*(4), 317-339, doi:http://dx.doi.org/10.1016/0032-0633(79)90110-7.

Scarf, F. L., R. W. Fredricks, D. A. Gurnett, and E. J. Smith (1978), Isee-C Plasma-Wave Investigation, *Ieee T Geosci Remote*, *16*(3), 191-195, doi:Doi 10.1109/Tge.1978.294544.

Séran, H. C., and P. Fergeau (2005), An optimized low-frequency three-axis search coil magnetometer for space research, *Rev Sci Instrum*, *76*(4), 044502, doi:doi:http://dx.doi.org/10.1063/1.1884026.

Shawhan, S., D. Gurnett, D. Odem, R. Helliwell, and C. Park (1981), The plasma wave and the quasi-static electric field instrument (PWI) for Dynamics Explorer-A, *Space Science Instrumentation*, *5*(4), 535-550.

Stone, R. G., et al. (1992), THE UNIFIED RADIO AND PLASMA-WAVE INVESTIGATION, *Astron. Astrophys. Suppl. Ser.*, *92*(2), 291-316.

Torbert, R. B., et al. (2016), The FIELDS Instrument Suite on MMS: Scientific Objectives, Measurements, and Data Products, *Space Sci Rev*, *199*(1), 105-135, doi:10.1007/s11214-014-0109-8.

Tumanski, S. (2007), Induction coil sensors—a review, *Measurement Science and Technology*, *18*(3), R31.

Underhill, C. R. (1910), *Solenoids Electromagnets and Electromagnetic Windings*, D. Van Nostrand Comapny, New York City.

Welsby, V. G. (1960), The theory and design of induction coils.

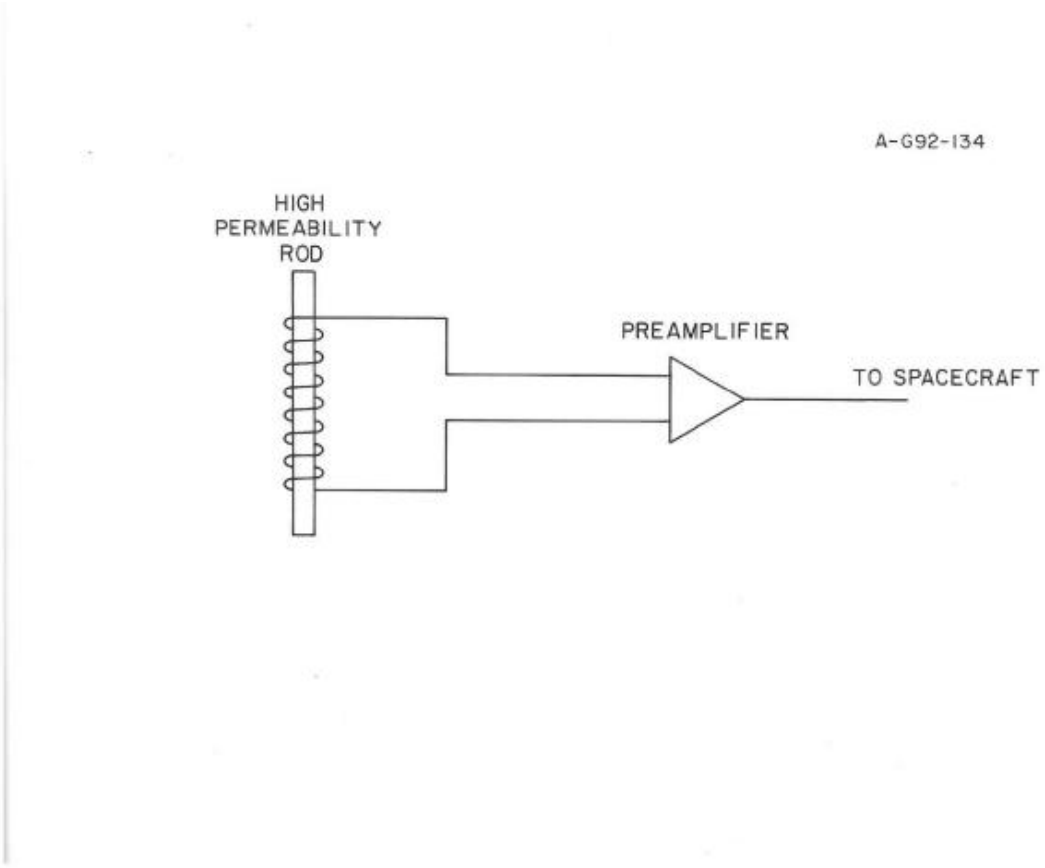

Figure 1. Sketch of basic design of a search coil magnetometer. Thousands of turns of wire wound on a high permeability core. The output of the coil is usually attached to a preamplifier, which amplifies the induced voltage and conditions the signal for transmission to the main electronics (usually a low frequency radio receiver).

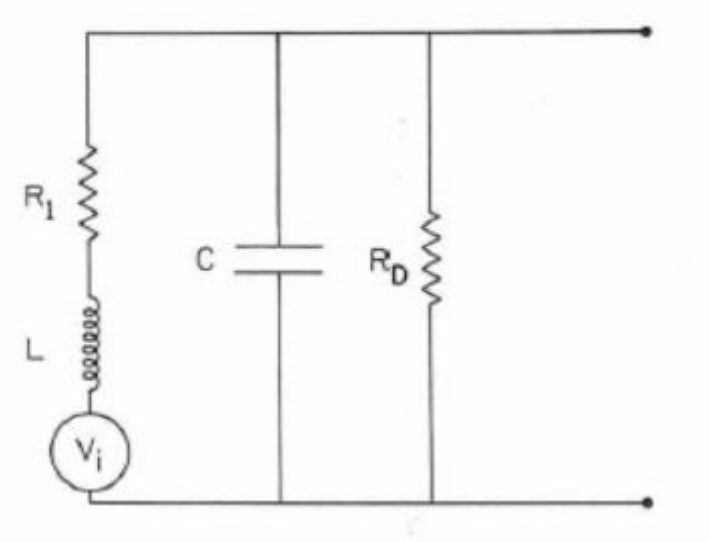

Figure 2. Equivalent circuit for a typical search coil magnetometer.

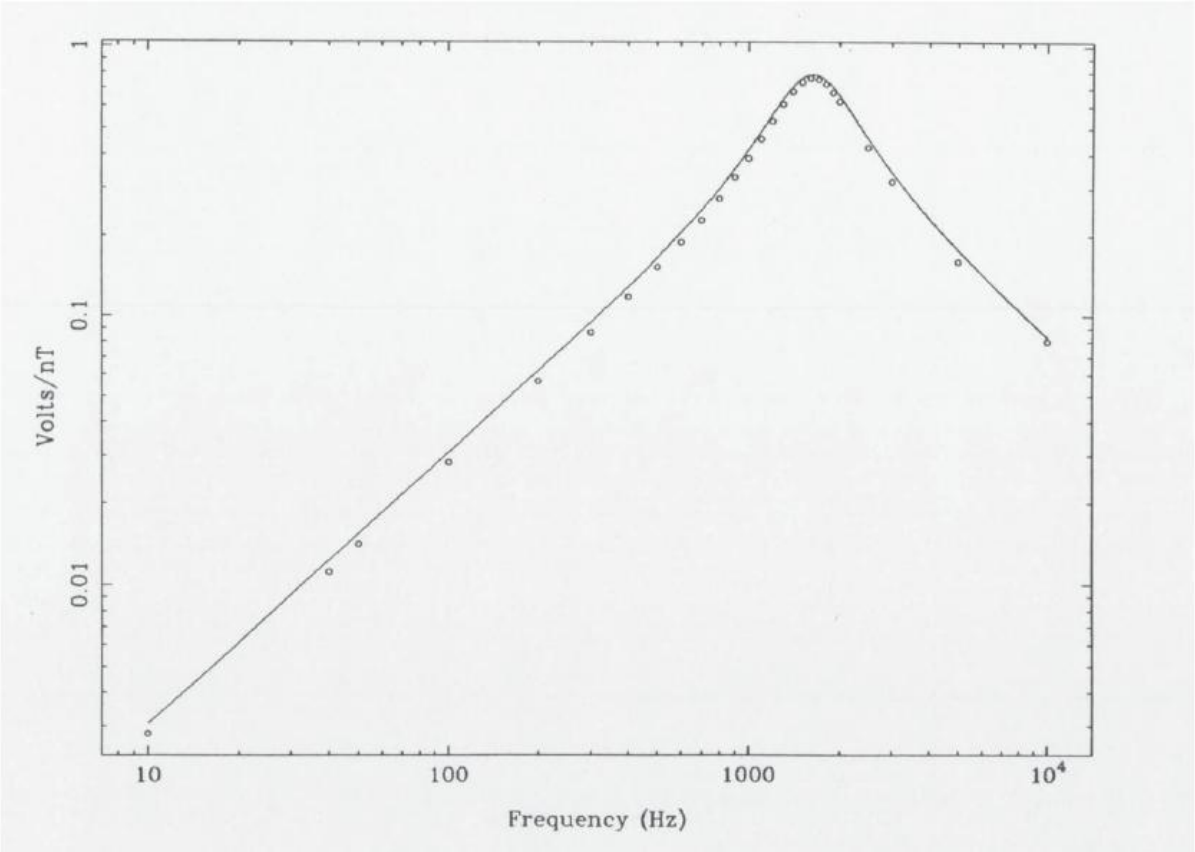

Figure 3. Comparison of the theoretical transfer function (Equation 5) for the Wind search coils (solid line) vs. measured transfer function (circles).

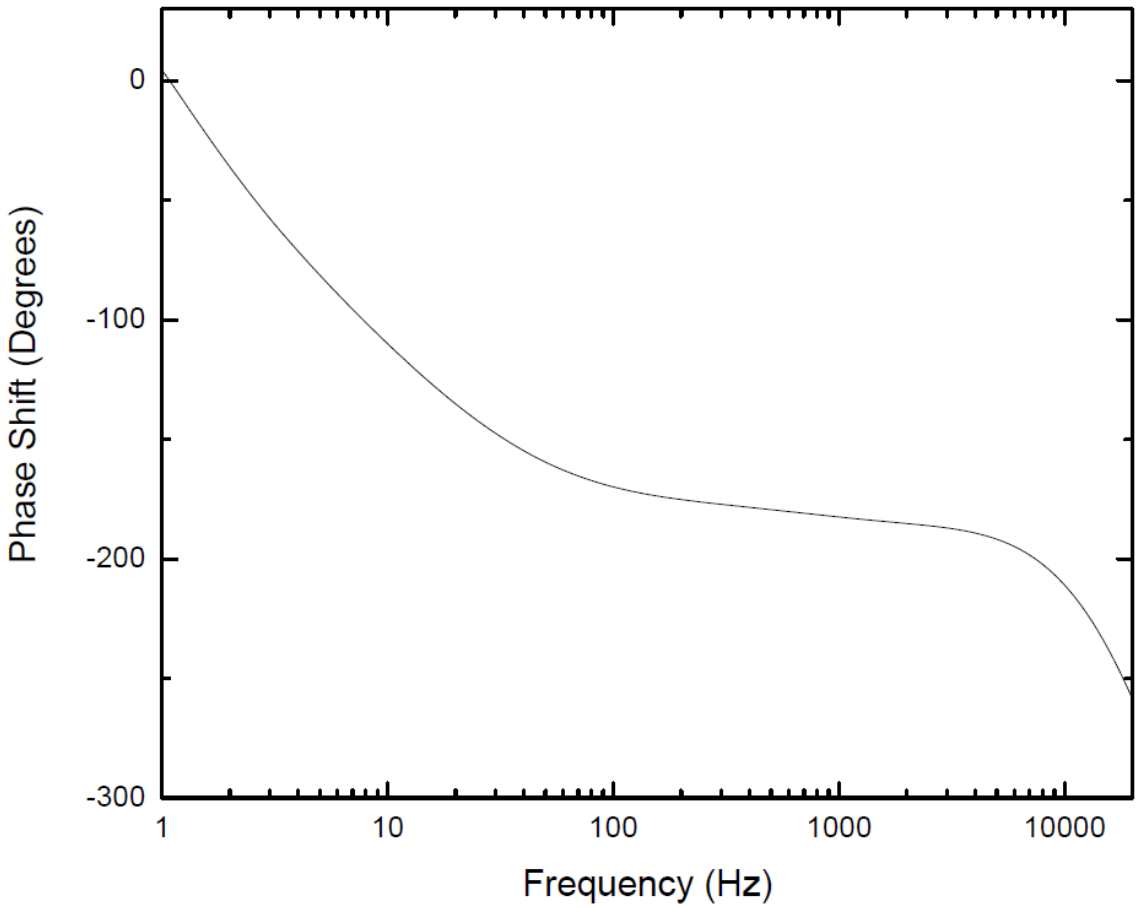

Figure 4. Relative phase response of the Van Allen Probe search coils.

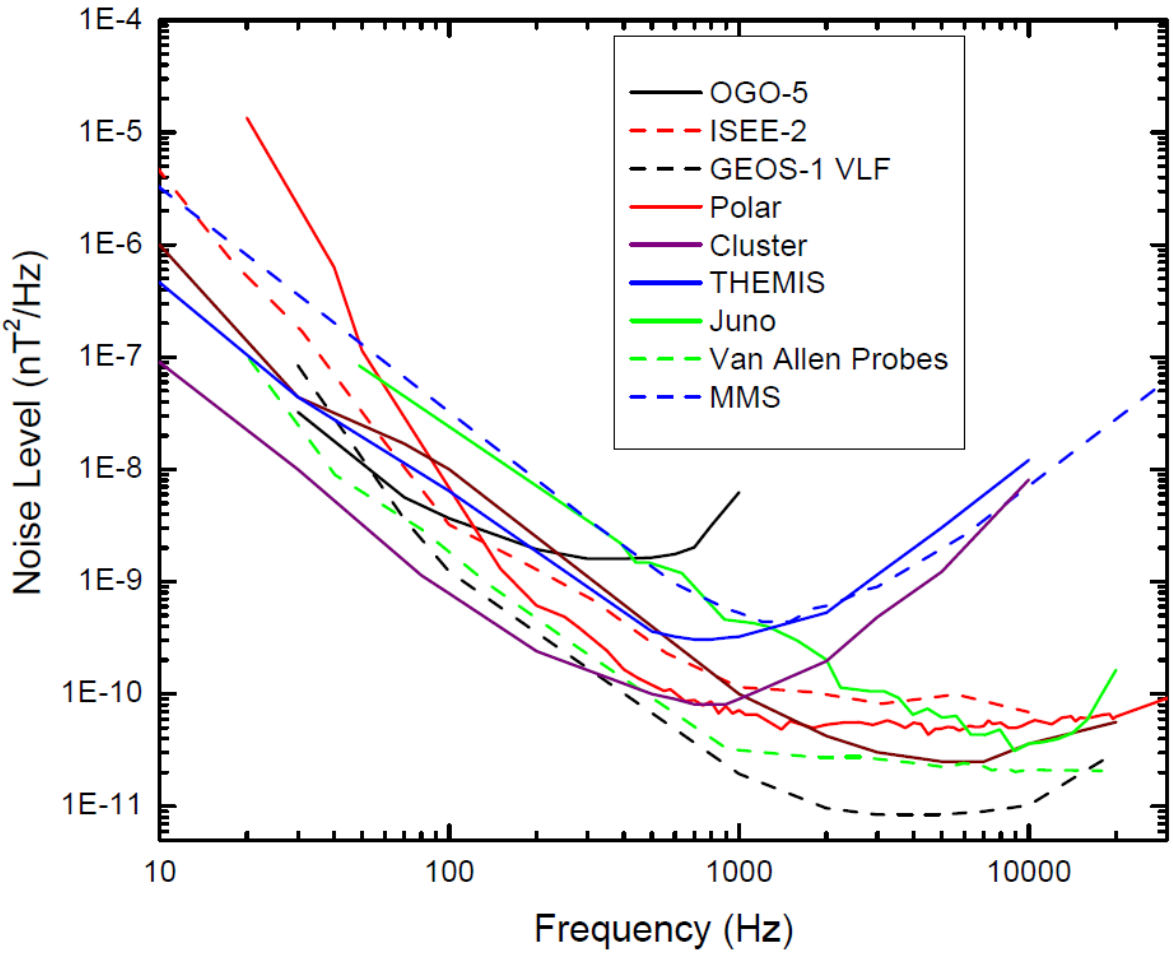

Figure 5. Comparison of the noise level of a number of different search coils, including OGO-5 (black line) [*Frandsen et al.*, 1969], ISEE-2 (red dashed line) [*Gurnett et al.*, 1978], GEOS-1 (black dashed line) [*S-300 Experimenters*, 1979], Polar (red line) [*Hospodarsky*, 1992], Cluster (purple line) [*Cornilleau-Wehrlin et al.*, 1997], THEMIS (blue line) [*Roux et al.*, 2008], Juno (green line), Van Allen Probes (green dashed line) [*Kletzing et al.*, 2013b], and MMS (blue dashed line) [*Le Contel et al.*, 2016].

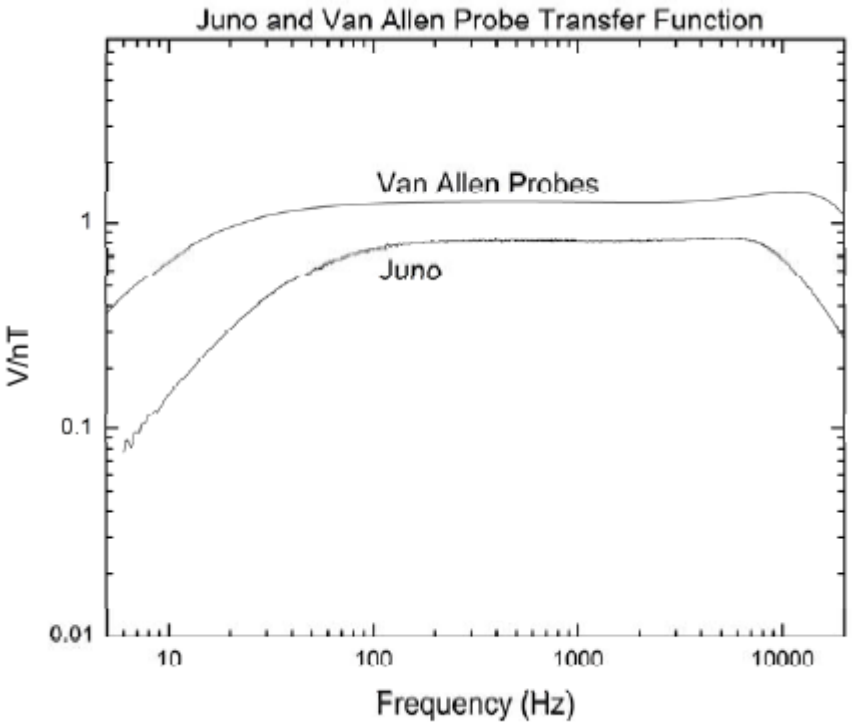

Figure 6. Transfer functions of the Juno and Van Allen Probes search coils.